Localized surface plasmon modes in a system of two interacting metallic cylinders

Viktoriia E. Babicheva,[1,2] Sergey S. Vergeles,[1,3,*] Petr E. Vorobev,[1,3] and Sven Burger[4]

[1]*Moscow Institute of Physics and Technology, Institutskij pereulok 9, 141700 Dolgoprudnyj, Moscow Region, Russia*
[2]*DTU Fotonik, Technical University of Denmark, Oersteds Plads 343, 2800 Kgs. Lyngby, Denmark*
[3]*Landau Institute for Theoretical Physics RAS, Kosygina 2, 119334 Moscow, Russia*
[4]*Zuse Institute Berlin, Takustraße 7, 14195 Berlin, Germany*
Corresponding author: vergeles@gmail.com

We study an optical response of a system of two parallel close metallic cylinders having nanoscale dimensions. Surface plasmon excitation in the gap between the cylinders is specifically analyzed. In particular, resonance frequencies and field enhancement were investigated as functions of geometrical characteristics of the system and ohmic losses in the metal. The results of numerical simulations were systematically compared with the analytical theory, obtained in the quasi-static limit. The analytical method was generalized in order to take into account the retardation effects. We also present the physical qualitative picture of the plasmon modes, which is validated by numerical simulations and analytical theory. © 2012 Optical Society of America

OCIS codes: 160.3918, 240.6680, 260.3910.

1. INTRODUCTION

Localized surface plasmon excitations in metal-dielectric systems of subwavelength size is a topic under intensive study during the last decade. Fabrication techniques of wire-grid polarizers [1,2], nanoantennas [3–7], and arrays of metallic particles [8–10] are rapidly improving. Optical properties of aggregates of metallic grains are very different from those of the separate grains. Field refraction by such systems possesses typical features, in particular a strong field enhancement in the gaps between closely located metallic particles leading to an increase of scattering and absorption in comparison with those for single grains. The resonance frequency of surface plasmons in the systems depends on both particle sizes and interparticle distances. It is red-shifted for modes with electric field polarization directed across the gaps between the grains and blue-shifted in the opposite case; see, e.g., experimental works [5,6] and numerical investigations [11–13]. The electric field enhancement inside the gaps under the resonance conditions can reach sufficient values, and one can use the effect to achieve Raman detection of single molecules placed into the gap [14,15].

One encounters difficulties trying to describe plasmon modes analytically since an exact solution is only possible for systems with very simple geometry. The geometry should allow us to use an appropriate coordinate system for which separation of variables in the Helmholtz equation is possible [16]. Among the systems are spherical metal particles [17], surface plasmon propagation in plane metal films [18], dielectric gaps in metallic cladding [19], and along nanowires [20]. Although the solutions for these systems are quite simple, they yield basic understanding of the fundamentals of the surface plasmon physics at nanoscales.

The problem of two particles (in particular cylinders) in the external field can be approximately solved using dipole-dipole approximation if the interparticle distance is much larger than their sizes. When the interparticle distance gets smaller, this approximation becomes inappropriate even for qualitative description of the system, and one should use multipole-multipole expansion technique [21]. There are some works that try to employ the multipole-multipole expansion technique in order to approach a system of two close metallic particles of more complex form [22] or a system of several particles [23] or metamaterials [24,25], which is associated with the calculation of the formally infinite series. The method has advantages for numerical simulation, whereas it does not allow us to establish qualitative properties of the plasmon modes in the systems, in particular their scaling behavior on the geometry of the system.

The problem can be simplified at scales less than the wavelength. In this case, the Helmholtz equation is reduced to the Laplace equation since retardation effects are negligible. This fact allows one to analytically solve the problem about surface plasmon mode structure for more complex systems such as two close spherical grains [26–28] and two close cylinders with circular cross section [29]. To analyze solutions, it is reasonable first to consider a qualitative picture [26,29] that describes the plasmon modes in the systems. The qualitative picture can be constructed applying the solution for surface plasmon propagation in a thin dielectric gap [19] to the gap between two granules.

In this paper, we investigate scattering of light by a system of two close parallel metallic cylinders. We sequentially compare the results of numerical simulations of the electromagnetic near field distribution with predictions of the theory [29] developed for the quasi-static (long wavelength) limit. Following [29], we present the qualitative picture of the surface plasmon resonance in the system in more details, and show its agreement with both analytical (in quasi-static limit) and numerical solution of Maxwell's equations.

One of the main flaws of the method employed in [29] is that it does not account for retardation effects, which means that its applicability diminishes with the increase of the system size. Moreover, it does not account for the radiation losses, which could be significant even for the small system, provided that the ohmic losses are small enough. In this paper, and it is its main point, we present the numerical results that on the one hand account for the retardation effects, and thus are applicable for the systems of any size and material constants, and on the other hand extend the analytical methods of [29] to account for the radiation losses explicitly. We verify the accuracy of our numerical calculations by systematically comparing their results to analytical ones in the appropriate limit of small system size. We also present the results of numerical simulations for the silver cylinders in the experimentally interesting region of frequencies and for realistic sizes (up to 100 nm), which is slightly beyond the scope of the analytical quasi-stationary method, which describes the picture only qualitatively. Silver is chosen since it is widely used in experimental works in nano-optics (see, e.g., [9,30]) due to its low ohmic losses.

2. PROBLEM FORMULATION

We examine scattering of an electro-magnetic plane wave by two close metallic cylinders under the conditions of surface plasmonic resonance. The size of the cylinders in cross-plane is assumed to be of the order or less than the wavelength. Figure 1 illustrates the system of two cylinders with circular cross sections together with the Cartesian coordinate system that we operate. The radii of both cylinders are equal to a, and the width of the gap between the cylinders is δ. We consider a particular case of TM-wave when the electric field of the incident wave is polarized along the line connecting the cylinders' axes. Such a choice is made because surface plasmon modes with red-shifted resonance frequencies and high local enhancement of the electric field in the gap between the cylinders [29] are achieved for this polarization only. The red shift corresponds to a high negative value of the dielectric constants contrast (permittivity ratio) $\varepsilon = \varepsilon_m/\varepsilon_d$, where ε_m and ε_d are the permittivities of the metal and the surrounding dielectric, respectively.

The complete system of Maxwell's equations can be reduced to the wave equation on the only nonzero magnetic field Z-component H,
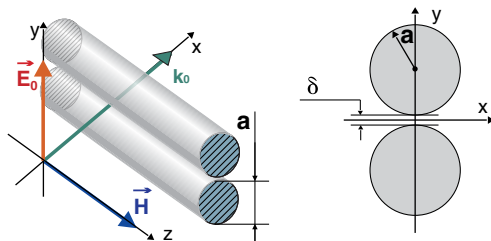
$$\operatorname{div} \frac{1}{\varepsilon(r)} \operatorname{grad} H + \frac{\omega^2}{c^2} H = 0, \qquad (1)$$

where ω is the frequency of the incident wave. We assume the magnetic permeability μ to be unity both in metal and in surrounded space. The electric field is orthogonal to OZ-axis; thus the problem becomes effectively two-dimensional. The electric field distribution can be restored as $E^\alpha = (ic/\omega\varepsilon(r))\eta_{\alpha\beta}\partial_\beta H$, where $\eta_{\alpha\beta}$ is two-dimensional antisymmetric tensor, $\eta_{xy} = 1$, and α, β runs values x, y.

The numerical simulations were performed with commercially available software JCMsuite [31]. The software solves Maxwell's equations based on a finite element method (FEM). It gives high advantages in simulations of structures with small curved elements. In particular, the package JCMsuite showed very good results in a benchmark simulation of plasmonic nanoantennas [32], which are similar to our structure. The simulations are challenging because of the narrow gap between cylinders. The studied system is under resonance condition and exhibits large field enhancement, so field distribution based adaptive meshing should be applied. An optimal number of refinement steps was found, as well as a number of points on circuits in the vicinity of the gap for the manual mesh specification. A solution convergence based on posteriori error estimation was examined in the same way as in [31] and [33].

For the modes under consideration, the magnetic field H is symmetric with respect to the axis OX of the system, and the electric field lines are normal to the axis. This fact allowed us to choose the computational domain that contains one-half of the system shown in Fig. 1 and perfect metal boundary conditions at the OX-axis.

Setting permittivity of surrounding medium $\varepsilon_d = 1$ in numerical simulations, we suppose that permittivity ratio is equal to complex metal permittivity and can be expressed as $\varepsilon = \varepsilon' + i\varepsilon''$; i.e., ε' is the real part of the permittivity and ε'' is the imaginary part.

In the following, we use the term "model" metal. By this we mean that we can arbitrarily assign any values to its permittivity at any wavelength in order to illustrate the dependence of certain quantities (e.g., resonance conditions, field enhancement factor) on the parameters of the system. Having understood the general properties of plasmon modes in such systems, we turn to investigation of the optical properties on silver cylinders. For silver, both the real ε' and the imaginary ε'' parts of the dielectric permittivity are functions of the wavelength λ, which dependencies can be extracted from [34].

3. ANALYTIC SOLUTION

If the cylinder radius a is much less than the wavelength in the outer space, $\sqrt{\varepsilon_d}ka \ll 1$, and the skin layer in the metal, $\sqrt{|\varepsilon_m|}ka \ll 1$, with k being the free space wavenumber, it is possible to develop an analytical solution. One can neglect retardation effects and assume $\omega = 0$ in Eq. (1), thus describing the system in the quasi-static approximation as a pair of cylinders in a homogenous external electric field. The solution of such a problem depends on frequency implicitly via metal permittivity $\varepsilon(\omega)$. This description is valid at distances close to the system, $r \ll \lambda/\sqrt{\varepsilon_d}$.

It is more convenient to use the electric field potential Φ instead of the magnetic field H in this approximation. The

Fig. 1. (Color online) Two close cylinders, coordinate system and field polarization.

electric field is $E = -\text{grad}\,\Phi$ in the case. The reason is that the qualitative physical picture of the surface plasmon oscillations has clear explanation in terms of the potential Φ. Maxwell's equations are reduced to quasi-static equation

$$\text{div}(\varepsilon(r)\text{grad}\,\Phi) = 0 \tag{2}$$

in the vicinity of the cylinders. Equation (2) reduces to the Laplace equation inside and outside the cylinders: $\Delta\Phi = 0$. The boundary conditions are the continuity of the potential and normal component of the electric displacement $\varepsilon(r)\partial_n\Phi$. The potential should tend to unperturbed external field potential far from the system; thus $\Phi \rightarrow -E_0 y$ when $r \gg a$, where E_0 is the electric field of the incident wave. Note here that the symmetry of the external field potential $-E_0 y$ in respect to OXZ-plane corresponds to the symmetry of potential in surface plasmons, which are realized at high negative permittivity ratio ε.

Equation (2) does not explicitly contain dependence on the frequency. The dependence of the scattering properties of the system stems from the dependence of the metal permittivity on the frequency. Thus, the most dependencies presented in this paper are given in terms of the real part ε' of the metal permittivity. Knowing dispersion of permittivity for a given metal, one can rewrite all the dependencies in terms of frequency. Here we note that the plots are not changed dramatically in this case, since the dependence of the metal permittivity is usually monotonic in the frequency domain under consideration.

In order to solve the above stated problem, we use the so-called bipolar coordinates system: two dimensionless coordinates ξ and η are related to the Cartesian coordinates as follows:

$$x = \frac{a\,\sinh \xi_0\,\sin \eta}{\cosh \xi - \cos \eta}; \qquad y = \frac{a\,\sinh \xi_0\,\sinh \xi}{\cosh \xi - \cos \eta}. \tag{3}$$

The lines $\xi = \pm\text{const}$ are the pairs of circles situated symmetrically in respect to OX-axis (see Fig. 1). By definition, ξ_0 corresponds to the cylinder surfaces; that is, $\sinh^2(\xi_0/2) = \delta/(4a)$. Reference system transformation (3) is a conformal map. The Laplace operator in bipolar coordinates is given by the following expression:

$$\nabla^2 \equiv \frac{1}{h^2(\xi, \eta)}\left(\frac{\partial^2}{\partial\xi^2} + \frac{\partial^2}{\partial\eta^2}\right), \tag{4}$$

where $h = a\,\sinh \xi_0/(\cosh \xi - \cos \eta)$ is the scaling function.

The partial solutions of the Laplace equation can be written as $e^{\pm n\xi}\cos n\eta$ or $e^{\pm n\xi}\sin n\eta$ in separated variables. In order to solve the problem of two cylinders in the external field, one has to expand the potential in terms of these partial solutions. Using the symmetry, we can write

$$\Phi^{\text{in}} = E_0 a \sum_0^\infty A_n e^{-n\xi}\cos n\eta; \qquad \xi > 0, \tag{5}$$

$$\Phi^{\text{out,ind}} = E_0 a \sum_1^\infty B_n \sinh n\xi \cos n\eta, \tag{6}$$

where Φ^{in} is the potential inside the cylinders and $\Phi^{\text{out,ind}}$ is the induced part of the potential outside the cylinders.

Coefficients A_n and B_n are to be found from the boundary conditions.

Now let us expand the potential of the external field $\Phi_0 \equiv -E_0 y$ in terms of partial solutions of the Laplace equation. Simple but cumbersome calculations give

$$\Phi_0 = -\text{sign}\xi E_0 a\,\sinh \xi_0\left(\sum_{n=1}^{+\infty} 2e^{-n|\xi|}\cos n\eta + 1\right). \tag{7}$$

The solution of the problem can be written explicitly ($n \geq 1$)

$$B_n = -\frac{2\,\sinh \xi_0(1 - \varepsilon)e^{-n\xi_0}}{\sinh n\xi_0(\varepsilon + \coth n\xi_0)}, \qquad A_n$$
$$= -\frac{2\,\sinh \xi_0 e^{n\xi_0}}{\sinh n\xi_0(\varepsilon + \coth n\xi_0)}. \tag{8}$$

For $n = 0$, the coefficients $B_0 = 0$, $A_0 = -\sinh \xi_0$.

It follows from Eq. (8) that the resonance occurs when permittivity contrast ε takes values

$$\varepsilon_n = -\coth n\xi_0. \tag{9}$$

Expression (6) allows one to calculate the amplitude of the electric field. Explicit expression for electric field components reads

$$E_x^{\text{ind}} = \left(\sinh \xi \sin \eta \frac{\partial}{\partial\xi} - \left(1 - \cosh \xi \cos \eta\right)\frac{\partial}{\partial\eta}\right)\frac{\Phi^{\text{ind,out}}}{a\,\sinh \xi_0}, \tag{10}$$

$$E_y^{\text{ind}} = -\left(\left(1 - \cosh \xi \cos \eta\right)\frac{\partial}{\partial\xi} + \sinh \xi \sin \eta \frac{\partial}{\partial\eta}\right)\frac{\Phi^{\text{ind,out}}}{a\,\sinh \xi_0}. \tag{11}$$

In what follows, we use these expressions to evaluate the electric field spatial distribution in the vicinity of the cylinders.

4. RESULTS FOR THE LIMIT OF CLOSE CYLINDERS

In this section, we analyze the limit of two close cylinders, when the width δ of the gap between the cylinders is small compared to the cylinder radius a; i.e., $\delta \ll a$. The condition means that the dimensionless parameter $\xi_0 \approx \sqrt{\delta/a} \ll 1$ in Eq. (3).

The resonance condition (9) becomes

$$\varepsilon_{\text{res}} = -\frac{1}{n}\sqrt{a/\delta} \tag{12}$$

with the limit $n \lesssim \sqrt{a/\delta}$. The result can be qualitatively explained as follows. The resonance condition enables the existence of standing surface plasmon waves in the flat region of the gap, which has the approximate length $\sim\sqrt{a\delta}$ [19]. This is a general point, which is valid in the case of two close metal spheres as well [26,27]. Expression (12) is valid until the

retardation effects become important at the scale $\sim\sqrt{a\delta}$; thus the applicability condition is $\sqrt{\varepsilon_m}k\sqrt{a\delta} \ll 1$.

Numerical simulations results for positions of the resonances are shown on Fig. 2 for two different levels of ohmic losses in metal. One can see maxima, which correspond to the resonances (9). The dependence of the position of the first resonance on the geometrical parameters of the system is plotted on Fig. 3; expression $\coth \xi_0$ tends to $(a/\delta)^{1/2}$ at small gap width.

We performed numerical simulations for silver cylinders using experimental values of permittivity [34] for silver. We chose the size of the system to be close and slightly below that experimentally achieved (see, e.g., [3]). Resonance permittivity (its real part) ratio as the function of geometrical parameters of the system is plotted in Fig. 3. Electric field enhancement in the center of the gap between the cylinders as a function of incident wavelength is plotted in Figs. 4 and 5. In Fig. 4, all curves correspond to the same value of the gap width $\delta = 3$ nm. In Fig. 5, all curves excepting that for $a = 15$ nm, $\delta = 1$ nm correspond to the same value of the ratio $\delta/a = 0, 1$. When comparing the plots from these figures with Fig. 2, one should bear in mind that the absolute value of the real part $|\varepsilon'|$ of the dielectric permittivity of silver is a monotonically increasing function of the wavelength λ. One can see that at most only the first two distinct resonance peaks can be observed for silver cylinders, due to the presence of ohmic losses that lead to broadening and overlapping of all the rest peaks. Total losses increase with the size of the system, due to increased radiation intensity. In Fig. 5, the local minimum near 430 nm and 400 nm of the enhancement factor in the case of cylinders with radii 100 nm and 200 nm, correspondingly, should be ascribed to retardation effects. The same concerns the local minimum near 500 nm for the curve corresponding to $a = 120$ nm in Fig. 4. For thinner cylinders, retardation does not lead to any qualitative effects. In fact, the form of the curve E_c^2/E_0^2 as a function of λ is independent of the absolute values of the cylinder radii a and the gap thickness δ in the quasi-static limit. It is a function of the ratio a/δ (or the parameter ξ_0) only. This can be perceived from the general properties of the Laplace equation, which solutions do not change after rescaling of the whole system. The curves are shifted to lower values of E_c^2/E_0^2 for large values of the
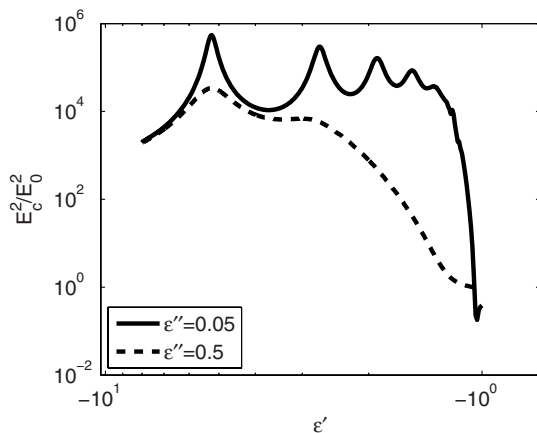
cylinders' radii due to radiation losses, the relative importance of which decreases with the wavelength λ [see Eq. (17) below].

Now let us examine in detail the enhancement of the electric field in the gap when the real part of permittivity contrast ε' is close to the first resonance position $\varepsilon_1 = -\sqrt{a/\delta}$. One can see that in the vicinity of the resonance, the contribution from the first harmonics in Eq. (6) is much larger than those from all the rest. It follows from the symmetry of the problem that electric field on the OXZ-plane is directed normal to the plane and is equal to

$$E_y = \frac{4(a/\delta)E_0}{\varepsilon - \varepsilon_1}\frac{x^2/a\delta - 1}{((x^2/a\delta)^2 + 1)^2}, \qquad (13)$$

where we have taken into account the fact that $\delta \ll a$. This expression is valid provided $kx \ll 1$. Electric field changes its sign at $x = l$, where

$$l = \sqrt{a\delta}, \qquad (14)$$

and this length should be interpreted as the mode size, i.e., wavelength of plasmon in flat dielectric gap with thickness δ between two bulk metal media [19].
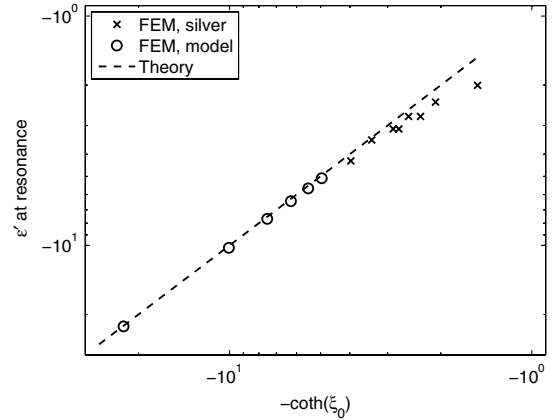

Fig. 3.   Value of real part of permittivity ε as a function of affinity of the cylinders for main resonance, $n = 1$. It was taken $a = 50$ nm, $\varepsilon'' = 0.6$, and $\lambda = 2\ \mu m$ in numerical simulations for model metal. For silver, $a = 15$ nm was taken.

Fig. 2.   Numerical simulation results for electric field enhancement in the center of the gap between the cylinders as a function of real part ε' of model metal permittivity. The wavelength is $\lambda = 2\ \mu m$, the radius of the cylinders is $a = 50$ nm, and the gap width is $\delta = 2$ nm.
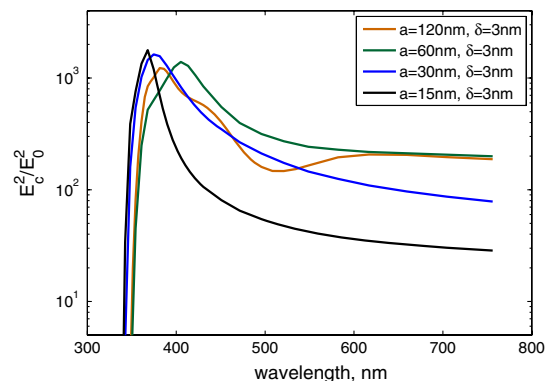

Fig. 4.   (Color online) Numerical simulation results for electric field enhancement in the center of the gap for silver cylinders as a function of wavelength for constant width gap $\delta = 3$ nm. Compare with Fig. 2.
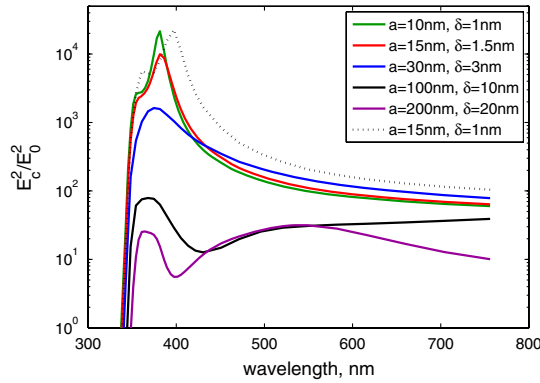
Fig. 5. (Color online) Numerical simulations results for electric field enhancement in the center of the gap for silver cylinders as a function of wavelength for constant ratio $a/\delta = 10$ (solid lines). Dashed line is given for comparison and corresponds to different ratio $a/\delta = 15$. Compare with Fig. 2.

Numerical simulation results for the mode size as a function of geometrical parameters of the system are shown in Fig. 6. The expression (15) is consistent with our qualitative explanation (12) and is valid under the same condition $\sqrt{\varepsilon_m}k\sqrt{a\delta} \ll 1$.

It follows from Eq. (13) that the field at the center of the gap is

$$E_c = -\frac{4}{\sinh^2\xi_0}\frac{E_c}{\varepsilon - \varepsilon_1} = -\frac{4a}{\delta}\frac{E_0}{\varepsilon - \varepsilon_1}. \tag{15}$$

The first representation in Eq. (15) is written for general case, whereas the second one is valid for the limit of closely located cylinders. At the resonance, i.e., real part $\varepsilon' = \varepsilon_1$, Eq. (15) is reduced to $E_c = -4E_0(a/\delta)/\varepsilon''$. The field enhancement at the resonance as a function of imaginary part of the permittivity contrast is shown in Fig. 7. The deviation of the enhancement factor in numerical simulations from the analytical prediction (15) at small ε'' is due to radiation losses that become important for these values of ε'', whereas law (15) accounts for ohmic losses in metal only. The radiation losses are determined mainly by the dipole radiation, since the size of the system is much less than the wavelength. The dipole moment of the
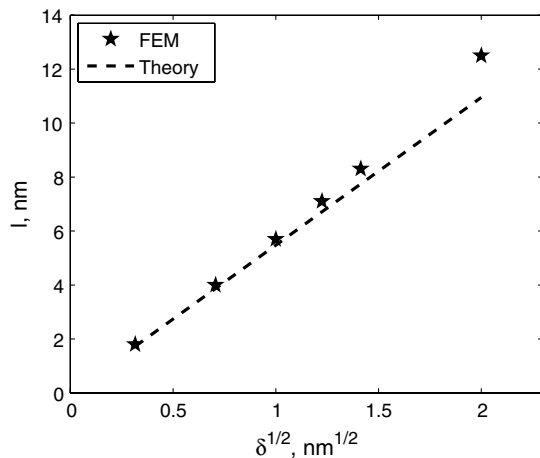

Fig. 7. Dependence of electric field enhancement on imaginary part ε'' of model metal permittivity in the first resonance. The wavelength is $\lambda = 2~\mu$m, the radius of the cylinders is $a = 50$ nm, and the gap width is $\delta = 1$ nm. The dotted line corresponds to law (17) at resonance in the pure quasi-static limit, and the dashed line accounts for radiative losses, which are given by Eq. (17).

system (per unit length) $d \sim a\delta E_c$ can be extracted from far asymptotics of the electric field (13). Radiation losses per unit length can be estimated as $I \sim \omega^3 d^2/c^2$. The ohmic losses in metal can be estimated by multiplying the dissipation ratio per unit volume $\sim \varepsilon''(E_c/\varepsilon')^2$ by the volume, occupied by the field $\sim a\delta$. Thus the dissipation rate (per unit length of cylinders) is estimated as $Q \sim \varepsilon''E_c^2\delta^2$. Expression (15) is valid provided $I \ll Q$, that is while $\varepsilon'' \gg (ka)^2$.

The field enhancement at the resonance in the gap between the cylinders as a function of geometrical parameters is plotted in Fig. 8. For model metal, we assume a wavelength of $\lambda = \mu$m, which means that the radiation losses are small compared to the ohmic ones. For silver cylinders, the deviation of the enhancement factor from law (15) is substantial. This is due to the fact that wavelength at the resonance frequency is not well above the size of the system.

At scales $x \gg \sqrt{a\delta}$, expression (13) gives the quadratic decay law of the electric field as a function of coordinate

$$E_y = -\frac{a\delta}{x^2}E_c. \tag{16}$$

Fig. 6. Dependence of mode size on geometrical parameters, for $\lambda = 2~\mu$m, $\varepsilon'' = 0.6$, $a = 30$ nm. Deviation from the dashed line corresponding to law (16) at large δ is due to contribution from nonresonance harmonics in expansion (12).
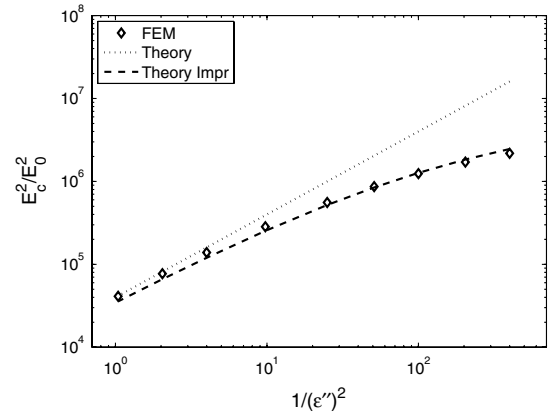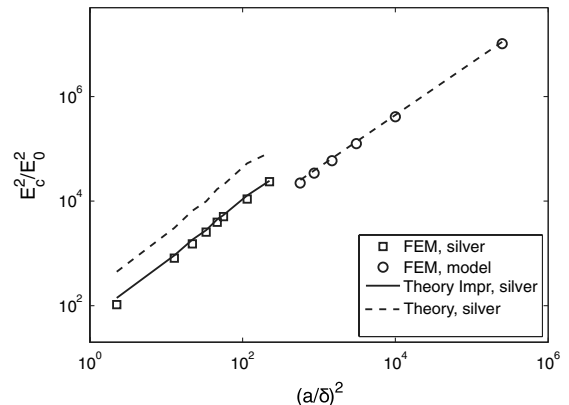

Fig. 8. Dependence of field enhancement factor in resonance on geometrical parameters. It was taken $a = 30$ nm, $\varepsilon'' = 0.6$, and $\lambda = 2~\mu$m in numerical simulations for model metal. For silver, $a = 15$ nm was taken. Dashed lines correspond to theory prediction (17) without taking into consideration radiation losses; the solid line takes the losses into account [see Eq. (17)].

The qualitative explanation of this law for scales $\sqrt{a\delta} \ll x \ll a$ is as follows. The potential difference $\Delta\Phi$ between the surfaces of the cylinders is constant at the scales, since the surface plasmon wavelength in the gap of thickness y is much larger than the typical x. Thus $E_y = \Delta\Phi/\Delta y$, where $\Delta y \approx x^2/a$ is the gap width at given x. The potential difference can be related to the electric field strength E_c at the center of the gap through the condition that the full surface charge on each cylinder is zero. The surface charge has different signs inside the flat region at distances $x < l$ and outside the region (the size of the mode). The electric field can be assumed to be uniform in Y-direction across the gap; thus $E_c l \sim -\int_l^a dx \Delta\Phi/\Delta y$. The value of this integral is mostly formed at lower limit, and finally one finds $\Delta\Phi \sim -E_c\delta$. To check the decay law (16) in numerical experiment, we chose an extremely small value of the gap to provide a large difference between scales l and a; the result is presented in Fig. 9.

Decaying law (16) for larger scales, $x \gg a$, corresponds to field of dipole $d = -2a^2 E_0/(\varepsilon - \varepsilon_1)$; the asymptotics is valid for any value of the ratio δ/a. Note that the dipole moment is formed at scales $x \sim a$, and the minor part of the total surface charge is involved in the process. In fact, the dipole moment can be estimated as the integral over the region $l \ll x \ll a$, $d \sim \int dx \Delta\Phi$. The integral is formed at distances $x \sim a$, where only the small part $\sqrt{\delta/a}$ of surface charge is located. The inner region does not give feasible contribution in d due to the small charge separation length.

One can improve Eq. (15) by taking into account the radiation losses. As a result, the resonance value of dielectric permittivity ε_1 [Eq. (9)] achieves imaginary negative contribution $i\varepsilon_1''$, $\varepsilon_1'' < 0$. The correction can be extracted from the condition that dipole radiation is equal to power supplied to the system from the external electric field provided Ohmic losses are zero, $I = W$. The intensity of the radiation is $I = (\pi c k^3/4)|d^2|$, and the power supplied to the system is $W = \omega E_0 \text{Im}[d]/2$, where E_0 is assumed to be real, and $\text{Im}[d]$ is the imaginary part of the dipole moment induced in the system. At resonance conditions, the dipole moment is pure imaginary; thus we find $d = (2i/\pi)E_0/k^2$. Comparing the result with Eq. (15), we obtain
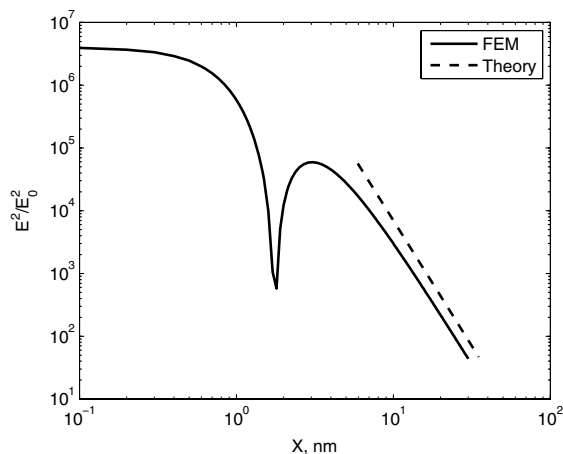
$$\varepsilon_1'' = -\pi k^2 a^2,$$

Fig. 9.   Field spatial dependence on the middle line between the cylinders. Parameters are $a = 30$ nm, $\delta = 0.1$ nm, $\varepsilon' = -17.4$, $\varepsilon'' = 0.6$, $\lambda = 2$ μm. Dashed line is asymptotics $E \propto 1/x^2$; see Eq. (16).

where ε_1' should be determined from Eq. (9). The correction is valid if $(ka)^2 \ll 1$ and is applicable for the arbitrary ratio of cylinders' radii and the intercylinder distance, including the case when $\delta \sim a$. In Figs. 7 and 9, theoretical curves that take into account the radiation correction (17) are presented. The curves fit numerical data quite well; thus the deviation of the data curve from the theoretical prediction [Eq. (15)] with pure real ε_1 should be assigned just to unaccounted radiation losses.

5. CONCLUSION

We have numerically investigated the distribution of the electro-magnetic field induced by the incident plane wave near a system of two closed parallel metallic cylinders of nanoscale dimensions modeled by Maxwell's equations. The comparison of the results of the numerical simulation with the analytical solution for the plasmon modes in the system governed by Maxwell's equations in the quasi-static limit showed agreement between these two approaches.

The position of the resonance is determined by the geometrical characteristics of the gap between the cylinders. Resonance corresponds to the existence of the standing wave inside the almost flat part of the gap, which can be thought of as a plane metal-dielectric-metal structure. Since the wavelength of the plasmon depends on its frequency (through permittivity of metal), there exist a set of resonance frequencies corresponding to the set of standing modes in the gap. Comparison with numerical simulations gives a good agreement, since the dimension of the gap is smaller than the size of the metallic granules, and the quasi-static approximation used in the analytical theory has high accuracy.

The analytically obtained [29] field enhancement factor in the center of the gap for the first resonance has also good agreement with that obtained numerically. It is determined both by ohmic losses in the metal and by radiative losses, with relative importance of the latter rising with the size of the system. We assumed the radii of the cylinders to be of the order of 100 nm, which is implemented in experiments [3]. The skin layer depth in metal is of the same order; thus the quasi-static approximation has some deviations from the exact solution of the Maxwell's equations.

Finally, we studied the dependence of the field enhancement for the case of silver cylinders with permittivity taken from experimental data. Our numerical simulations for such systems showed that only the ohmic losses are reasonable, and only the first two resonances can be really observed.

REFERENCES

1. M. Suzuki, A. Takada, T. Yamada, T. Hayasaka, K. Sasaki, E. Takahashi, and S. Kumagai, "Low-reflective wire-grid polarizers with absorptive interference overlayers," Nanotechnology **21**, 175604 (2010).
2. Y. Ekinci, H. H. Solak, C. David, and H. Sigg, "Bilayer Al wire-grids as broadband and high-performance polarizers," Opt. Express **14**, 2323–2334 (2006).

3. R. M. Bakker, H-K. Yuan, Z. Liu, V. P. Drachev, A. V. Kildishev, V. M. Shalaev, R. H. Pedersen, S. Gresillon, and A. Boltasseva, "Enhanced localized fluorescence in plasmonic nanoantennae," Appl. Phys. Lett. **92**, 043101 (2008).

4. J. Zhang, Y. Fu, M. H. Chowdhury, and J. R. Lakowicz, "Metal-enhanced single-molecule fluorescence on silver particle monomer and dimer: coupling effect between metal particles," Nano Lett. **7**, 2101–2107 (2007).

5. D. Bloemendal, P. Ghenuche, R. Quidant, I. G. Cormack, P. Loza-Alvarez, and G. Badenes, "Local field spectroscopy of metal dimers by TPL microscopy," Plasmonics **1**, 41–44 (2006).

6. P. K. Jain, W. Huang, and M. A. El-Sayed, "On the universal scaling behavior of the distance decay of plasmon coupling in metal nanoparticle pairs: a plasmon ruler equation," Nano Lett. **7**, 2080–2088 (2007).

7. J. Berthelot, A. Bouhelier, C. Huang, J. Margueritat, G. Colas-des-Francs, E. Finot, J-C. Weeber, A. Dereux, S. Kostcheev, H. I. E. Ahrach, A-L. Baudrion, J. Plain, R. Bachelot, P. Royer, and G. P. Wiederrecht, "Tuning of an optical dimer nanoantenna by electrically controlling its load impedance," Nano Lett. **9**, 3914–3921 (2009).

8. Z.-K. Zhou, M. Li, Z.-J. Yang, X.-N. Peng, X.-R. Su, Z.-S. Zhang, J.-B. Li, N.-C. Kim, X.-F. Yu, L. Zhou, Z.-H. Hao, and Q.-Q. Wang, "Plasmon-mediated radiative energy transfer across a silver nanowire array via resonant transmission and subwavelength imaging," ACS Nano **4**, 5003–5010 (2010).

9. S. A. Maier, P. G. Kik, H. A. Atwater, S. Meltzer, E. Harel, B. E. Koel, and A. A. G. Requicha, "Local detection of electromagnetic energy transport below the diffraction limit in metal nanoparticle plasmon waveguides," Nat. Mater. **2**, 229–232 (2003).

10. A. W. Sanders, D. A. Routenberg, B. J. Wiley, Y. Xia, E. R. Dufresne, and M. A. Reed, "Observation of plasmon propagation, redirection and fan-out in silver nanowires," Nano Lett. **6**, 1822–1826 (2006).

11. J. Clarkson, J. Winans, and P. Facuhet, "On the scaling behavior of dipole and quadrupole modes in coupled plasmonic nanoparticle pairs," Opt. Mater. Express **1**, 970–979 (2011).

12. I. Romero, J. Aizpurua, G. W. Bryant, and F. J. Garcia De Abajo, "Plasmons in nearly touching metallic nanoparticles: singular response in the limit of touching dimers," Opt. Express **14**, 9988–9999 (2006).

13. V. Amendola, O. M. Bakr, and F. Stellacci, "A study of the surface plasmon resonance of silver nanoparticles by the discrete dipole approximation method: effect of shape, size, structure and assembly," Plasmonics **5** 85–97 (2010).

14. Y. Cheng, M. Wang, G. Borghs, and H. Chen, "Gold nanoparticle dimers for plasmon sensing," Langmuir **27**, 7884–7891 (2011).

15. G. Haran, "Single-molecule Raman spectroscopy: a probe of surface dynamics and plasmonic fields," Acc. Chem. Res. **43**, 1135–1143 (2010).

16. P. M. Morse and H. Feshbach, *Methods of Theoretical Physics. Part II* (McGraw-Hill, 1953).

17. A. D. Boardman and B. V. Paranjape, "The optical surface modes of metal spheres," J. Phys. F **7**, 1935–1945 (1977).

18. D. Y. Fedyanin, A. V. Arsenin, V. G. Leiman, and A. D. Gladun, "Backward waves in planar insulator-metal-insulator waveguide structures," J. Opt. **12**, 015002 (2010).

19. I. P. Kaminow, W. L. Mammel, and H. P. Weber, "Metal-clad optical waveguides: analytical and experimental study," Appl. Opt. **13**, 396–405 (1974).

20. C. A. Pfeiffer, E. N. Economou, and K. L. Ngai, "Surface polaritons in a circularly cylindrical interface: surface plasmons," Phys. Rev. B **10**, 3038–3051 (1974).

21. P. Nordlander, C. Oubre, E. Prodan, K. Li, and M. I. Stockman, "Plasmon hybridization in nanoparticle dimers," Nano Letters **4**, 899–903 (2004).

22. S. V. Zhukovsky, C. Kremers, and D. N. Chigrin, "Plasmonic rod dimers as elementary planar chiral meta-atoms," Opt. Lett. **36**, 2278–2280 (2011).

23. M. Hentschel, D. Dregely, R. Vogelgesang, H. Giessen, and N. Liu, "Plasmonic oligomers: the role of individual particles in collective behavior," ACS Nano **5**, 2042–2050 (2011).

24. J. Petschulat, C. Menzel, A. Chipouline, C. Rockstuhl, A. Tünnermann, F. Lederer, and T. Pertsch, "Multipole approach to metamaterials," Phys. Rev. A **78**, 043811 (2008).

25. D. N. Chigrin, C. Kremers, and S. V. Zhukovsky, "Plasmonic nanoparticle monomers and dimers: from nano-antennas to chiral metamaterials," Appl. Phys. B: Lasers Opt. **105**, 81–97 (2011).

26. V. Lebedev, S. Vergeles, and P. Vorobev, "Giant enhancement of electric field between two close metallic grains due to plasmonic resonance," Opt. Lett. **35**, 640–642 (2010).

27. V. V. Klimov and D. V. Guzatov, "Strongly localized plasmon oscillations in a cluster of two metallic nanospheres and their influence on spontaneous emission of an atom," Phys. Rev. B **75**, 24303 (2007).

28. M. H. Davis, "Two charged spherical conductors in a uniform electric field: forces and field strength," Q. J. Mech. Appl. Math. **17**, 499–511 (1964).

29. P. E. Vorobev, "Electric field enhancement between two parallel cylinders due to plasmonic resonance," J. Exp. Theor. Phys. **110**, 193–198 (2010).

30. A. M. Michaels, J. Jiang, and L. Brus, "Ag nanocrystal junctions as the site for surface-enhanced Raman scattering of single rhodamine 6G molecules," J. Phys. Chem. B **104**, 11965 (2000).

31. J. Pomplun, S. Burger, L. Zschiedrich, and F. Schmidt, "Adaptive finite element method for simulation of optical nano structures," Phys. Status Solidi B **244**, 3419–3434 (2007).

32. J. Hoffmann, C. Hafner, P. Leidenberger, J. Hesselbarth, and S. Burger, "Comparison of electromagnetic field solvers for the 3D analysis of plasmonic nanoantennas," Proc. SPIE **7390**, 73900J (2009).

33. S. Burger, R. Köhle, L. Zschiedrich, W. Gao, F. Schmidt, R. März, and C. Nölscher, "Benchmark of FEM, waveguide and FDTD algorithms for rigorous mask simulation," Proc. SPIE **5992**, 599216 (2005).

34. P. B. Johnson and R. W. Christy, "Optical constants of the noble metals," Phys. Rev. B **6**, 4370–4379 (1972).